Acta Geodyn. Geomater., Vol. 22, No. 3 (219), 291–302, 2025
DOI: 10.13168/AGG.2025.0020
journal homepage: https://www.irsm.cas.cz/acta

ORIGINAL PAPER

CHARACTERIZING THE SEASONAL LOADING DEFORMATION IN NORTH CHINA USING GNSS AND SURFACE LOADING MODELS

Xin WANG *, Lijun ZHANG, Guorui GENG, Chenxi QIN, Detang RAN, Fei WANG and Huimei WANG

The Third Exploration Team of Shandong Coalfield Geologic Bureau, Taian 271000, China

Corresponding author's e-mail: 15621525515@163.com

ARTICLE INFO

Article history:
Received 2 April 2025
Accepted 24 June 2025
Available online 3 July 2025

Keywords:
Crustal anisotropy
Moho and Conrad discontinuities
Common Conversion Point (CCP) stacking
410 km and 660 km discontinuities
Receiver function
Southeast Asia tectonics

ABSTRACT

The North China (NC) has suffered irreversible land subsidence in specific regions as a result of groundwater storage depletion. Investigating the influence of surface mass loading on seasonal deformation is essential for isolating accurate tectonic deformation linked to uplift and subsidence. This study utilized data from the Global Navigation Satellite System (GNSS) and Surface Loading Models (SLM) derived from the German Research Centre for Geosciences (GFZ) and the International Mass Loading Service (IMLS), covering the period from January 2011 to March 2023, to investigate the impacts of hydrological loading (HYDL), atmospheric loading (ATML), and non-tidal ocean loading (NTOL) on seasonal deformation in NC. The results indicated that the average root mean square (RMS) reduction value was -2.74 %, 5.9 %, and 1 % after deducting the deformation attributed to HYDL, ATML, and NTOL based on GFZ, respectively. Conversely, the average RMS reduction value from IMLS was 0.99 %, 5.6 %, and 1 %, respectively. Furthermore, the average annual amplitudes and phases in the seasonal deformations induced by ATML and GNSS time series were 4.7 mm and 175°, and 4.6 mm and 138°, respectively, indicating that the ATML can serve as a principal driving force for GNSS seasonal deformation in comparison of HYDL and NTOL. Additionally, we assessed the effect of surface mass loading on velocity and its uncertainty estimated from GNSS time series using the combination of white noise and flicker noise models, the results demonstrated that the average velocity and its uncertainty was 0.04 mm/a before and after SLM correction, revealing that that surface mass loading has a negligible influence on velocity and its uncertainty in NC.

1. INTRODUCTION

The North China (NC) region, recognized as the political and cultural center of China, serves as a vital economic hub and a principal grain production region. This region is comprised of Beijing, Tianjin, Hebei, and Shanxi, as well as the Inner Mongolia Autonomous Region (Wu et al., 2015; Liu et al., 2022). The massive exploitation of coal mines and groundwater for agricultural irrigation and domestic water use has resulted in considerable land subsidence in North China (e.g., Cangzhou, Hengshui) in recent years, which is attributed to the redistribution of surface mass loading (Zhang et al., 2025). The Earth is recognised as an elastic body, with deformation owing to uplift and subsidence being markedly affected by the redistribution of surface mass loading linked to non-tidal ocean loading (NTOL) (Haritonova et al., 2021), atmospheric loading (ATML) (Martens et al., 2020; Hohensinn et al., 2024), and hydrological loading (HYDL) (Chanard et al., 2014; Sauveur et al., 2024). A thorough comprehension of the impacts of HYDL, ATML, and NTOL on GNSS time series is crucial for isolating non-tectonic deformation. Consequently, investigating the seasonal deformation related to changes in surface mass loading in North China is of great significance for accurately determining tectonic deformation and elucidating land subsidence mechanisms, which are vital for the rational development of groundwater and sustainable urban construction.

The seasonal deformation yielded by ATML, HYDL, and NTOL can be measured using Global Navigation Satellite System (GNSS) (Xue et al., 2021; Wang et al., 2025) and Gravity Recovery and Climate Experiment (GRACE) along with GRACE Follow-On (GRACE-FO) (Heki et al., 2023). Additionally, these deformations can be effectively characterized by surface loading models (SLM) (Niu et al., 2022). Numerous studies have concentrated on characterizing the effects of ATML, HYDL, and NTOL at both global and regional scales through the integration of GNSS, GRACE/GRACE-FO, and SLM (Su et al., 2021; Liang et al., 2021; Crossley et al., 2023; Zhang et al., 2023). Quiete a few researchers have investigated the impact of ATML on seasonal variations in GNSS time series (He et al., 2022; Gobron et al., 2021; Li et al., 2024) revealing markedly greater magnitudes in high-latitude regions

Cite this article as: Wang X, Zhang L, Geng G, Qin C, Ran D, Wang F, Wang H: Characterizing the seasonal loading deformation in North China using GNSS and surface loading models. Acta Geodyn. Geomater., 22, No. 3 (219), 291–302, 2025. DOI: 10.13168/AGG.2025.0020

compared to low-latitude locations. A host of studies have shown a strong correlation between GNSS time series and the seasonal deformations induced by HYDL in specific regions, particularly in Amazon Basin (Ferreira et al., 2021), California (Carlson et al., 2022), and Yunnan (Jiang et al., 2021), where significant seasonal variations in continental water storage. Many studies have confirmed that the deformations caused by NTOL are confined to 2 mm in the inland region (Van Dam et al., 2012). In general, seasonal deformation resulting from the redistribution of surface mass loading can account for ~50 % of the annual amplitude variation in the GNSS time series under ideal conditions, and less than 20 % in horizontal deformation (Li et al., 2024).

Numerous researches have conducted the surface mass changes and their driving factors using GNSS, GRACE/GRACE-FO, and SLM data in North China (Wang et al., 2017; Jiang et al., 2024; Wang et al., 2023). Feng et al. (2022) proposed that ATML is a primary factor affecting the vertical GNSS seasonal deformation in North China. Li et al. (2020) and Liu et al. (2014) demonstrated that the seasonal deformation acquired from GNSS shows a good agreement with GRACE data, particularly when the combined impacts of ATML and NTOL (GAC solutions) are incorporated into the GSM solutions. Owing to the limitations in temporal and spatial resolution of GRACE/GRACE-FO, the SLM is more suitable for investigating seasonal deformation related to the redistribution of surface mass loading, as it can effectively represent large-scale surface mass loading signals and precisely capture local details in small-scale areas. Moreover, significant gaps exist in GRACE/GRACE-FO data, particularly between the years 2017 and 2018. More importantly, the difference in input data and assimilation methods employed by various institutions may lead to diverse effects of ATML, HYDL, and NTOL on GNSS seasonal deformation. Consequently, the selection of suitable SLM data sourced from diverse institutions is crucial for correcting seasonal variations in vertical GNSS time series within a certain region. In this study, we utilized the GNSS and different SLM data to investigate seasonal loading deformation in North China. Our research primarily focused on two major aspects: (1) Which SLM data has the most significant impact on the seasonal deformation of GNSS time series in North China? (2) Which sort of surface mass loading (ATML, HYDL, NTOL) predominantly influences seasonal deformation in North China?

2. DATA PROCESS AND METHODS

2.1. VERTICAL GNSS TIME SERIES DATA

We performed an investigation of seasonal deformation utilizing vertical GNSS time series over the period from January 2011 to March 2023 in North China, which is obtained from the GNSS data product service platform of China Earthquake Administration (http://www.cgps.ac.cn). Figure 1 illustrates the spatial distribution of 31 GNSS stations situated in North China. The GAMIT/GLOBK software was carried out to process the GNSS data. Initially, the unconstrained daily GNSS solutions were calculated for 31 stations using GAMIT software, encompassing station coordinates, satellite orbits, and zenith tropospheric delays. The primary strategies for processing are as follows: 1) the influences of polar tides, earth tides, and ocean tides, owing to Earth's rotation axis and gravitational pull of the moon and sun, were corrected using the corresponding models of IERS2010, FES2004, and IERS03, respectively; 2) The antenna offsets of GNSS receivers were calibrated utilizing the latest satellite and antenna absolute phase center correction model. Finally, the daily solutions produced by GAMIT software were ultimately transformed into the ITRF 2014 using a seven parameters transformation method. More information about GNSS data processing can be refer to Zhao et al. (2015).

It is unavoidable that offsets, outliers, and missing data present in the vertical GNSS time series. Therefore, it is indispensable to preprocess the vertical GNSS time series before conducting seasonal deformation analysis. The primary strategies employed for preprocessing in this study as follows: (1) Outliers were identified and removed from GNSS time series based on the interquartile range rule method (Suraci et al., 2025; Zhou et al., 2025); (2) Offsets resulting from the GNSS antenna changes, earthquakes, and other factors such as multipath effects, as well as variations in the reference frames employed during data processing, were rectified using least squares fitting method (Bevis et al., 2014; Huang et al., 2025); (3) We adopted the GNSS Missing Data Interpolation (GMIS) Software, developed by Liu et al. (2018), to resolve the issue of missing data. This dynamic spatial-temporal interpolation method utilizes a kriging Kalman filter, exhibiting remarkable efficacy in addressing continuous and random data discontinuities derived from GNSS network time series, this approach is extensively applied for gap-filling in missing GNSS time series (Peng et al., 2024; Tang et al., 2023). Figure 2 depicts the position offset correction, outlier removal, and interpolation results at the HECT station. As shown in Figure 2d, the interpolated data have a strong consistency with the GNSS time series, indicating distinct seasonal variations.

2.2. SURFACE LOADING MODEL DATA

The Earth's surface exhibits an elastic response to the redistribution of surface mass loading linked to HYDL, ATML, and NTOL, revealing significant seasonal deformations observed by GNSS stations. To quantify these effects, two principal modelling approaches are typically employed: the load Green’s function was developed by Farrell based on Longman’s Earth load theory (Farrell, 1972; Longman, 1963). This method computes surface deformation by convolution integrals applied to the Green's function. The spherical harmonic function

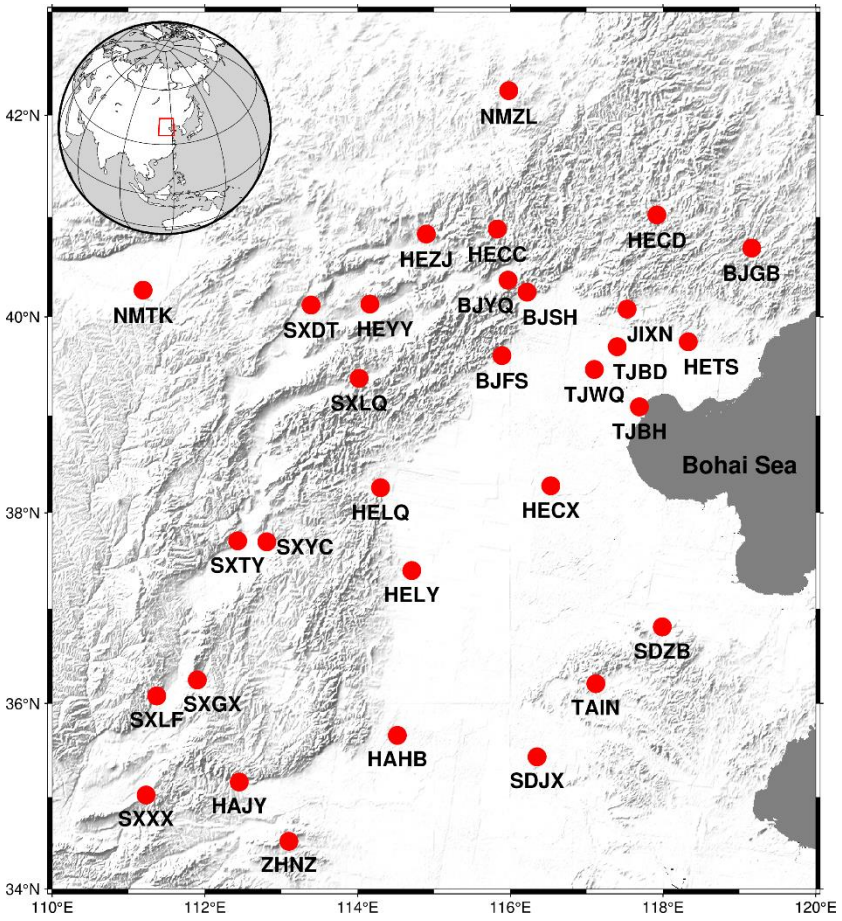

Fig. 1 Spatial distribution of 31 GNSS stations located in North China. The red dots represent GNSS stations.

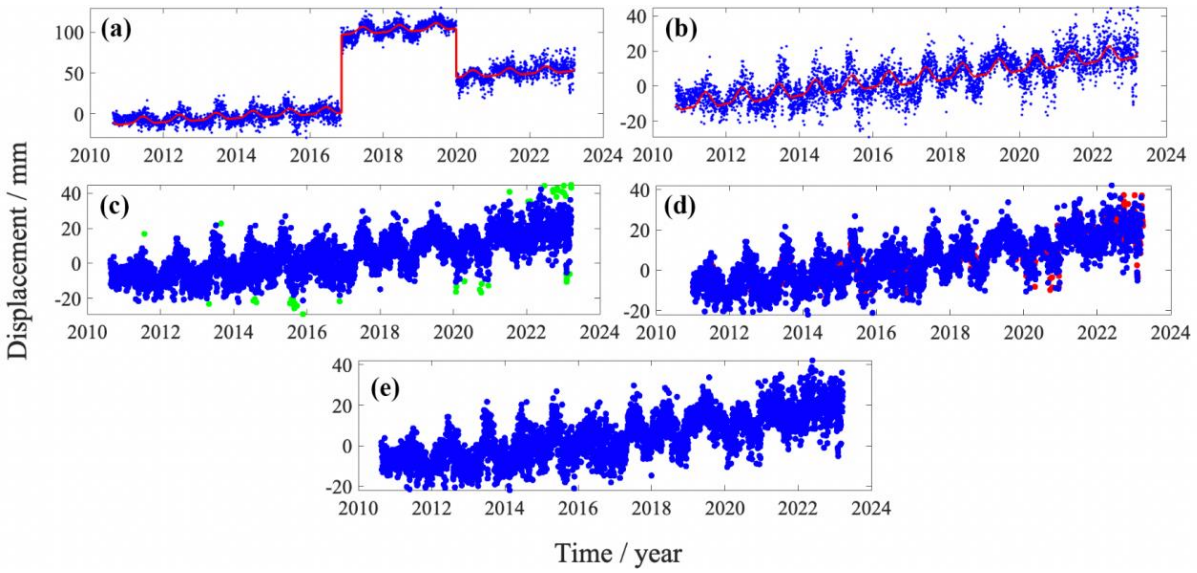

Fig. 2 Processing of vertical GNSS time series at the HECT station. (a), (b) represents before and after position offset correction, respectively ; (c), (d) represents origin GNSS time series and GMIS interpolation results, respectively; (e) represents outlier removal. The blue dot represents the original vertical GNSS time series, whereas the red line represents the vertical GNSS time series modeled by the least squares fitting method, and the green and red dots represents the outlier of GNSS vertical time series and interpolation data, respectively

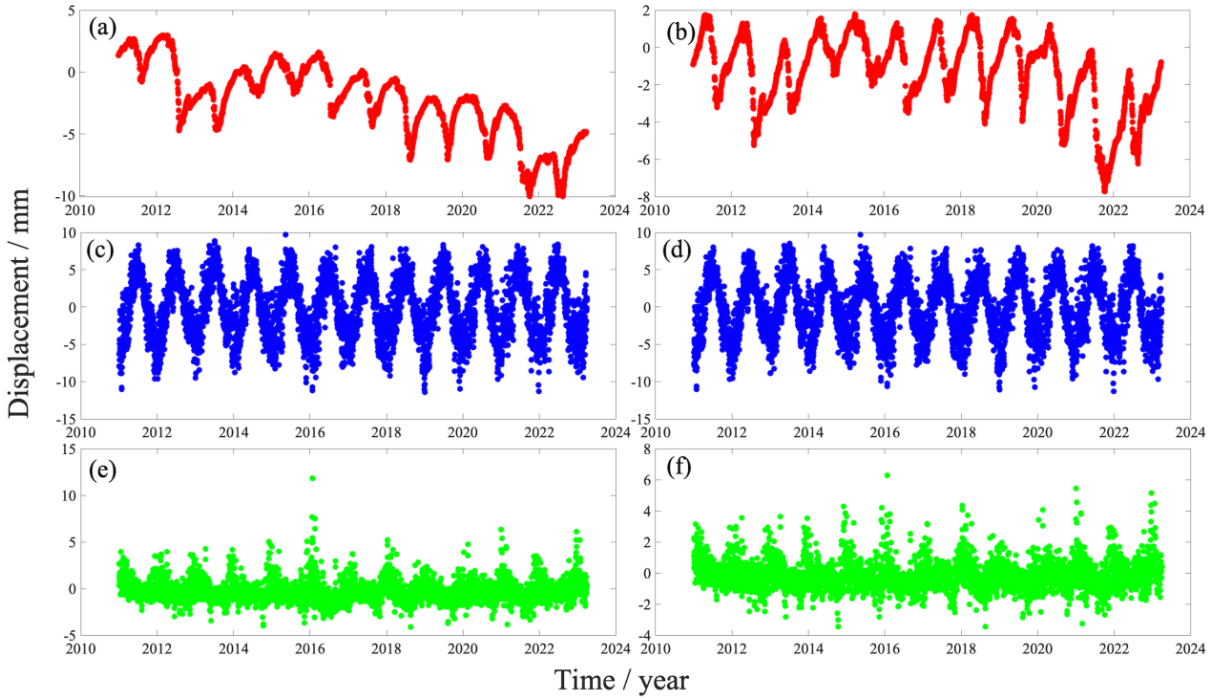

Fig. 3 The surface mass loading time series supplied by GFZ and IMLS at HECT station: (a), (c), (e) represents the HYDL, ATML, NTOL deformation from GFZ, respectively; (b), (d), (f) represent the HYDL, ATML, NTOL deformation from IMLS, respectively

method (Wang et al., 2014) is employed to decompose the global mass load into spherical harmonics. The surface mass loading deformation in the topocentric coordinate system is obtained by integrating and summing the spherical harmonic domains according to the latitude and longitude of the station, while applying Farrell's definition of load Love numbers. In this study, SLM data from the German Research Centre for Geosciences (GFZ) and the International Mass Loading Service (IMLS) were adopted to evaluate seasonal deformations resulting from HYDL, ATML, and NTOL effects. The SLM data from the GFZ are modeled using the Green's function method. The HYDL deformations derived from the Land Surface Discharge Model (LSDM) model (Dill et al., 2008), with a temporal and spatial resolution of 0.5°×0.5°×24h, primarily encompass soil moisture, river and lake water content, and snow water equivalent. The ATML and NTOL deformations were calculated using the European Centre for Medium-Range Weather Forecasts (ECMWF) model and Max Planck Institute Ocean Model (MPIOM) (Marsland et al., 2003), with a temporal and spatial resolution of 0.5°×0.5°×3h, respectively. The HYDL, ATML, and NTOL deformation based on GFZ in relation to the GNSS stations in North China, are acquired by interpolating the global grid data through the bilinear method. The SLM data supplied by the IMLS are constructed by the spherical harmonic function method. The HYDL deformation from the IMLS is computed using the MERRA2 (Modern-Era Retrospective Analysis for Research and Applications, version 2) model (Gelaro et al., 2017), with a temporal and spatial resolution of 2′×2′×3h, capturing soil moisture, canopy moisture, and snow water content. The ATML and NTOL deformation is computed using the MERRA2 model and the MPIOM06 model (Dobslaw et al, 2007), respectively, with a temporal and spatial resolution of 2′×2′×3h. To align the temporal resolution of the GNSS observation data, the original SLM data with a temporal resolution of 3h were averaged to a daily resolution. Figure 3 depicts the HYDL, ATML, and NTOL deformation at the HECT station, as supplied by GFZ and IMLS, indicating significant seasonal variations. Notably, the HYDL deformation signifies land subsidence, presumably associated with groundwater exploitation (Zhang et al., 2025).

$$y(t_i) = a + b*t_i + c*\sin(2\pi t_i + \varphi_1) + \\ + d*\sin(4\pi t_i + \varphi_2) + v_i \quad (1)$$

Where t_i represents the time epoch of GNSS observation; the coefficients a and b represents the initial position and linear trends velocity that quantify the rate of long-term change at GNSS station, respectively; c and φ_1 represents the amplitudes and phase of annual, respectively; d and φ_2 represents the amplitudes and phase of semi-annual, respectively; v_i represents fitting residuals.

2.3. CONSISTENCY ANALYSIS METHOD

We performed the LSF method to eliminate the linear trend of the GNSS time series at 31 GNSS stations in North China before assessing the impact of surface mass loading (HYDL, ATML, and NTOL) on

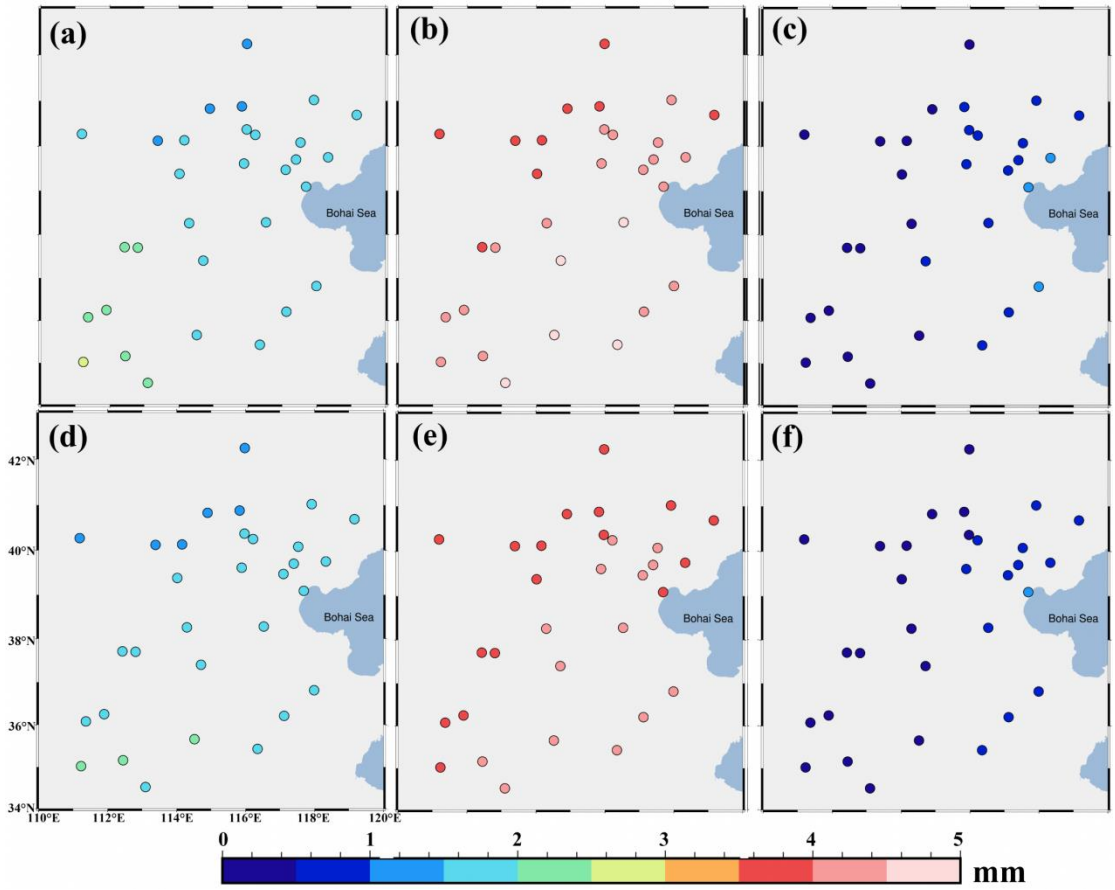

Fig. 4 RMS values of the seasonal deformation derived from SLM data. (a), (b), (c) represents the HYDL, ATML, NTOL deformation provided by GFZ; (d), (e), (f) represents the HYDL, ATML, NTOL deformation provided by GFZ.

the seasonal changes in vertical GNSS time series. This data preprocessing guarantees that subsequent analyses concentrate exclusively on seasonal deformation, excluding long-term tectonic deformation.

To quantify the consistency between the seasonal deformation developed from GNSS and SLM data, we employ the following equation (Pan et al., 2016; Gu et al., 2017; Hu et al., 2025).

$$RMS\left(GNSS\right)=\frac{\sqrt{\sum_{i=1}^{n}x\left(i\right)-\frac{\sum_{i=1}^{n}x\left(i\right)}{n}}}{n-1} \tag{2}$$

$$RMS_{reduction}=\frac{RMS\left(GNSS\right)-RMS\left(GNSS-SLM\right)}{RMS\left(GNSS\right)}\times 100\% \tag{3}$$

Where $x\left(i\right)$ represents the observation value of the GNSS station on the i day in North China, $RMS\left(GNSS\right)$ and $RMS\left(GNSS-SLM\right)$ represents the RMS value of the vertical GNSS time series as well as the RMS value after removing the HYDL, ATML, and NTOL deformations from vertical GNSS time series, respectively. If $RMS_{reduction}$ is positive, it signifies that surface mass loading correction can reduce the RMS value of the vertical GNSS time series, the bigger the value, the more effective the correction. Conversely, if $RMS_{reduction}$ is negative, it indicated that the surface mass loading correction will increase the RMS value of the vertical GNSS time series.

3. RESULTS AND DISCUSSION

3.1. COMPARISON OF SEASONAL DEFORMATION USING GNSS AND SLM

In general, the RMS value of seasonal deformations yielded by HYDL, ATML, and NTOL is an effective measure for assessing the extent of surface mass loading effects on the Earth's crust, revealing that the scatter and amplitude of seasonal variations of surface mass loading. These effects are essential for understanding how environmental mass redistributions affect GNSS observations, especially in the North China region, which offers high-resolution vertical GNSS time series. Figure 4 illustrates the RMS values of seasonal deformations acquired from SLM data, which is supplied by the GFZ and IMLS, revealing that ATML exerts the significant impact on seasonal deformation in North China, with RMS values ranging from 3.84 mm to

Table 1 Annual phase (unit: °) and amplitude (unit: mm) of GNSS and SLM time series.

Station	GNSS	GFZ_ HYDL	IMLS_ HYDL	GFZ_ ATML	IMLS_ ATML	GFZ_ NTOL	GFZ_ NTOL
BJFS	149.1/4.6	69.4/1.5	97.1/1.8	175.7/5.1	175.6/4.9	43.7/0.2	73.6/0.1
BJGB	149.6/4.5	63.0/1.4	94.6/1.6	175.3/4.6	174.4/4.5	30.3/0.5	58.3/0.2
BJSH	129.1/3.3	67.9/1.4	95.4/1.7	174.9/4.9	174.7/4.7	41.7/0.2	70.7/0.1
BJYQ	129.8/4.4	67.0/1.4	94.9/1.7	174.2/4.8	173.8/4.5	43.1/0.2	77.9/0.1
HAHB	149.6/5.2	66.3/2.3	95.4/1.8	178.2/5.7	178.2/5.4	85.6/0.1	131.6/0.1
HAJY	135.8/5.0	71.9/2.4	98.2/1.9	176.5/5.2	176.4/4.9	124.9/0.1	157.0/0.2
HECC	126.2/3.3	62.4/1.3	94.8/1.5	172.6/4.5	172.0/4.2	44.2/0.2	87.4/0.1
HECD	126.4/3.6	61.6/1.4	93.4/1.5	174.3/4.7	174.0/4.4	35.6/0.3	51.9/0.2
HECX	111.1/4.9	73.0/1.7	97.8/1.8	177.8/5.5	177.7/5.1	42.6/0.3	50.9/0.3
HELQ	153.8/5.2	72.4/1.7	96.4/1.9	175.8/5.2	175.7/5.0	63.3/0.1	116.7/0.1
HELY	146.4/4.8	70.1/1.8	96.6/1.9	177.1/5.5	177.0/5.2	64.9/0.2	111.7/0.01
HETS	151.5/4.3	68.8/1.6	98.7/1.6	176.8/4.9	176.8/4.7	32.4/0.6	39.3/0.4
HEYY	133.1/4.2	64.9/1.3	97.7/1.7	172.4/4.5	171.9/4.2	58.6/0.1	121.9/0.1
HEZJ	146.4/3.8	61.1/1.2	97.0/1.5	172.2/4.5	171.6/4.1	51.2/0.1	110.1/0.1
JIXN	143.3/4.1	67.3/1.5	98.3/1.7	176.1/5.0	176.0/4.8	36.0/0.4	48.1/0.2
NMTK	119.0/5.8	61.8/1.8	104.8/1.6	171.7/4.5	171.0/4.1	95.0/0.1	154.9/0.1
NMZL	115.4/3.1	51.1/1.1	98.9/1.2	170.9/4.2	169.9/3.8	45.2/0.1	105.2/0.1
SDJX	161.0/5.0	62.7/2.2	92.6/1.8	179.3/5.7	179.4/5.4	68.5/0.2	94.7/0.2
SDZB	115.8/3.9	69.8/2.0	91.6/1.8	178.8/5.2	178.9/5.0	43.8/0.5	53.3/0.4
SXDT	100.6/4.9	64.3/1.3	99.3/1.6	171.9/4.4	171.3/4.1	67.2/0.1	135.5/0.1
SXGX	158.9/5.8	76.0/2.0	99.4/2.0	174.7/4.9	174.3/4.5	118.3/0.1	156.4/0.1
SXLF	153.7/4.7	76.2/2.0	101.7/1.9	174.6/4.9	174.3/4.5	126.3/0.1	159.6/0.2
SXLQ	126.1/3.7	71.3/1.5	97.3/1.8	173.1/4.6	172.5/4.3	61.5/0.1	122.4/0.1
SXTY	144.5/4.5	76.4/1.8	99.7/1.9	173.5/4.7	173.1/4.4	94.5/0.1	148.4/0.1
SXXX	158.4/5.2	73.0/2.6	101.2/1.9	175.8/5.1	175.4/4.7	138.2/0.1	162.7/0.2
SXYC	144.8/4.7	76.5/1.8	98.1/1.9	173.8/4.7	173.6/4.4	88.9/0.1	143.9/0.1
TAIN	137.6/4.7	68.5/2.0	92.9/1.8	178.9/5.5	178.9/5.2	53.1/0.3	69.9/0.2
TJBD	133.0/4.4	67.8/1.5	99.4/1.7	176.8/5.1	176.7/4.9	36.1/0.4	46.9/0.3
TJBH	77.0/5.8	69.4/1.7	97.5/1.6	177.2/4.8	177.1/4.5	32.7/0.7	38.3/0.5
TJWQ	186.3/1.6	69.8/1.6	99.2/1.7	176.9/5.2	176.9/5.0	37.2/0.4	48.8/0.3
ZHNZ	167.1/5.4	64.8/2.6	94.8/1.8	177.9/5.6	177.7/5.2	125.5/0.1	155.6/0.2

4.61 mm (GFZ), and 3.63 mm to 4.45 mm (IMLS), averaging 4.18 mm and 4.00 mm, respectively, the RMS values of ATML deformation at coastal stations located in Jiaodong and Liaodong Peninsula are lower than those of inland stations owing to the ocean's reverse barometer effect. Conversely, NTOL exhibits the least effect on seasonal deformation in North China, with average RMS values under 1 mm (GFZ: 0.65 mm; IMLS: 0.58 mm), but it exceeds 1 mm at specific GNSS stations adjacent to the Bohai Sea, presumably due to localized oceanic influences. The RMS values of HYDL vary from 1.36 mm to 2.71 mm (GFZ) and 1.25 mm to 2.05 mm (IMLS), with averages 1.84 mm and 1.74 mm, respectively.

To further elucidate the seasonal signals, amplitudes and phases of annual in GNSS time series and surface mass loading deformation supplied by GFZ and IMLS were calculated using the LSF method, and the results are presented in Table 1. The GNSS time series in North China display annual amplitudes between 3.1 and 5.8 mm (average: 4.6 mm) and annual phases between 77° and 186° (average: 138°). For ATML, annual amplitudes based on GFZ range from 4.2 mm to 5.7 mm (average: 5.0 mm) with annual phases spanning from 170.9° to 179.3° (average: 175.4°), whereas annual amplitudes yielded by IMLS vary from 3.8 mm to 5.4 mm (average: 4.7 mm) and annual phases from 170° to 179.4° (average: 175°). The close alignment of annual amplitudes from ATML estimation between GFZ and IMLS, along with their resemblance to GNSS annual amplitudes, implying that ATML is a primary factor influencing GNSS seasonal variations in North China. The amplitude and phase of annual in ATML deformation acquired from GFZ and IMLS show negligible discrepancies in comparison of GNSS time series. For HYDL, annual amplitudes of HYDL deformation are consistent at 1.7 mm for both GFZ and IMLS. However, the annual phases varied markedly, measuring 67.9° and 97°, respectively, indicating discrepancies in the modeled HYDL deformation based on varying SLM data. The annual amplitudes of NTOL deformation are minimal (GFZ: 0.23 mm; IMLS: 0.17 mm).

Figure 5 depicts vertical GNSS time series alongside the associated SLM deformation, which is a composite of HYDL, ATML, and NTOL deformation from IMLS at stations (HELQ, HETS, SXGX, SXXX). Both datasets exhibit obvious seasonal oscillations, with vertical GNSS time series

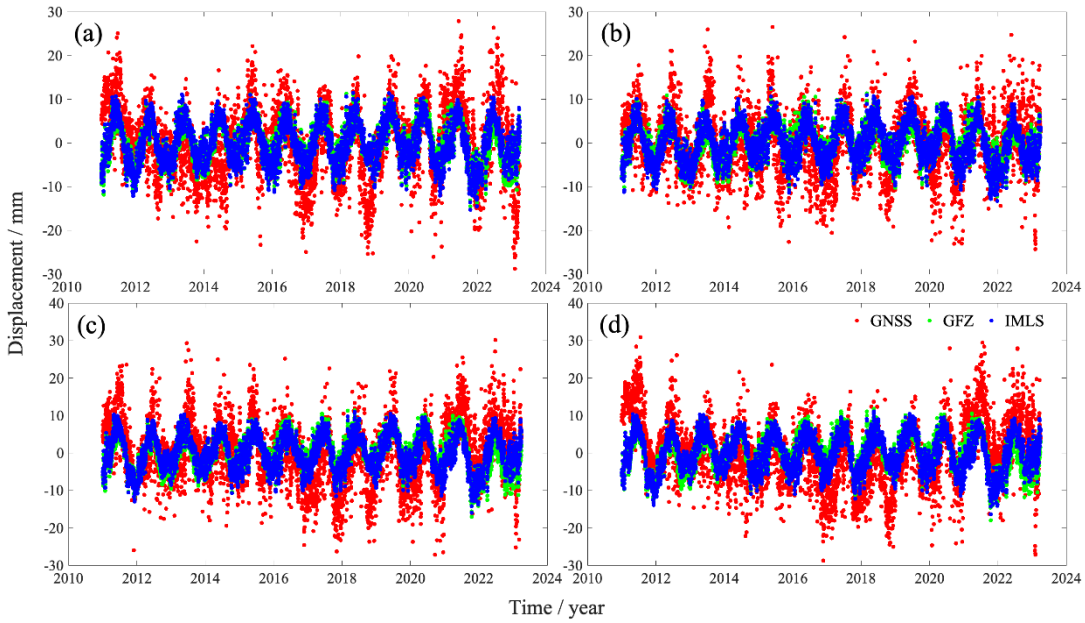

Fig. 5 Comparison of seasonal deformation derived from GNSS, GFZ, and IMLS at some GNSS station (a) HELQ, (b) HETS, (c) SXGX, (d) SXXX.

Table 2 RMS reduction value of the vertical GNSS time after deducting the deformation induced by HYDL, ATML, and NTOL provided by GFZ and IMLS (unit: %).

Station	GFZ_ HYDL	IMLS_ HYDL	GFZ_ ATML	IMLS_ ATML	GFZ_ NTOL	IMLS_ NTOL
BJFS	-4.09	-0.99	7.23	7.30	0.73	0.98
BJGB	-3.16	1.20	9.38	9.33	-0.11	0.95
BJSH	-1.41	0.51	0.49	0.91	1.28	1.36
BJYQ	-1.08	1.62	4.97	5.39	1.18	1.30
HAHB	-4.18	-0.72	6.84	6.82	0.96	1.08
HAJY	-5.29	1.94	5.76	5.89	1.03	1.09
HECC	-0.84	1.58	2.41	3.09	1.17	1.27
HECD	0.70	2.58	2.29	3.06	0.90	1.06
HECX	-3.38	-2.10	-0.22	-0.01	0.46	0.45
HELQ	0.48	2.77	10.82	10.96	0.51	0.80
HELY	-3.58	-1.62	6.72	6.82	1.04	1.20
HETS	-2.60	1.55	10.04	10.18	-0.38	0.24
HEYY	-3.03	3.25	6.99	7.40	0.95	1.16
HEZJ	-5.47	0.50	6.95	7.25	0.88	1.11
JIXN	0.02	0.24	5.56	5.85	0.74	1.05
NMTK	2.04	5.58	4.84	5.20	0.86	0.95
NMZL	-2.85	1.15	0.55	1.40	1.19	1.24
SDJX	-4.18	-0.53	10.74	10.89	0.78	1.01
SDZB	-0.89	0.11	-1.14	-0.81	1.88	1.90
SXDT	-1.37	2.56	-0.50	0.01	0.71	0.70
SXGX	-6.63	1.40	14.51	14.33	0.68	0.96
SXLF	-8.82	-0.67	7.79	7.81	0.95	1.11
SXLQ	-3.37	0.97	2.77	3.22	1.08	1.14
SXTY	-6.43	1.32	7.69	7.84	0.95	1.14
SXXX	-8.06	0.48	10.89	10.86	0.96	1.17
SXYC	-3.47	2.07	9.59	9.80	0.86	1.10
TAIN	1.36	3.55	6.19	6.62	1.08	1.25
TJBD	0.58	1.11	4.46	4.88	1.12	1.35
TJBH	-2.04	-2.66	-2.65	-2.41	1.40	1.26
TJWQ	-1.87	-2.21	0.63	0.59	0.18	0.20
ZHNZ	-2.12	4.18	11.94	12.20	0.51	0.70

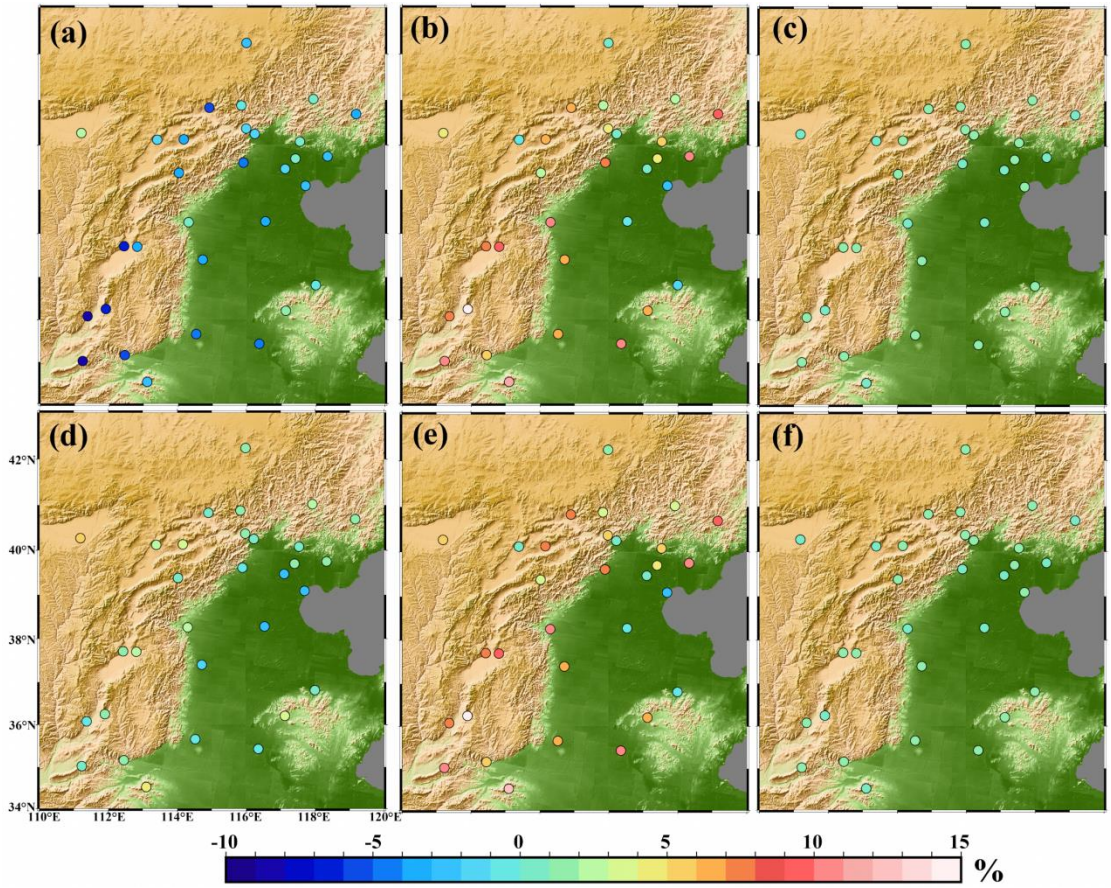

Fig. 6 RMS reduction results of the vertical GNSS time after deducting the deformation yielded by surface mass loading. (a), (b), and (c) represents the HYDL, ATML, NTOL correction based on GFZ, respectively; (d), (e), and (f) represents the HYDL, ATML, NTOL correction based on IMLS, respectively.

varying between -20 mm and 20 mm and SLM deformation ranging from -10 mm to 10 mm. This discrepancy indicates that SLM captures significant seasonal signals, it does not entirely account for the observed GNSS variability. Unmodeled groundwater changes and other effects associated with the thermal expansion of bedrock may elucidate the seasonal deformation observed in GNSS (Jiang et al., 2018). These findings highlight ATML's predominant impact on GNSS seasonal deformations in North China.

3.2. CONSISTENCY ANALYSIS OF THE SEASONAL DEFORMATION DERIVED FROM GNSS AND SLM

To quantitatively evaluate the relationship between SLM deformation and GNSS time series, we assessed their consistency using equation 3 outlined in Section 2.4. This equation quantifies the reduction in RMS after removing the SLM deformation from vertical GNSS time series, offering a metric to assess the effect of HYDL, ATML, and NTOL on GNSS seasonal signals. Figure 6 presents the results, which are summarized in Table 2, providing a comprehensive comparison at 31 GNSS stations in North China.

For ATML, the RMS reduction values from GFZ range from -2.7 % to 14.5 % (average: 5.9 %), whereas those from IMLS vary from -2.4 % to 14.3 % (average: 5.6 %). Figure 6e demonstrates that ATML positively decreases RMS value at 28 stations (90 % of total stations), indicating a strong corrective influence on GNSS seasonal variations at most stations in North China. For HYDL, the RMS reduction value from GFZ and IMLS range from -0.7 % to 5.6 %, and - 8.8 % to 2 %, with average of 0.99 % and -2.74 %, respectively. Figure 6d shows the RMS reduction value after HYDL deformation correction derived from GFZ were negative at most stations (25), accounting for 81 % of total stations, whereas the RMS reduction value from IMLS, accounting for 26 % of all stations, implying that HYDL can increase the RMS value of GNSS seasonal deformation at most stations in North China. Figure 6c illustrates that NTOL corrections from IMLS consistently yield positive RMS reduction (average: 1.0 %) at all stations. Overall, the deformation linked to ATML exhibits the highest agreement with GNSS time series when compared to HYDL and NTOL, indicating that the applicability of the surface mass loading corrections for the seasonal deformation of GNSS stations differs between regions. Additionally, the results indicated that significant discrepancies among the effect of HYDL from GFZ and IMLS in North China, owing to different modeling approaches,

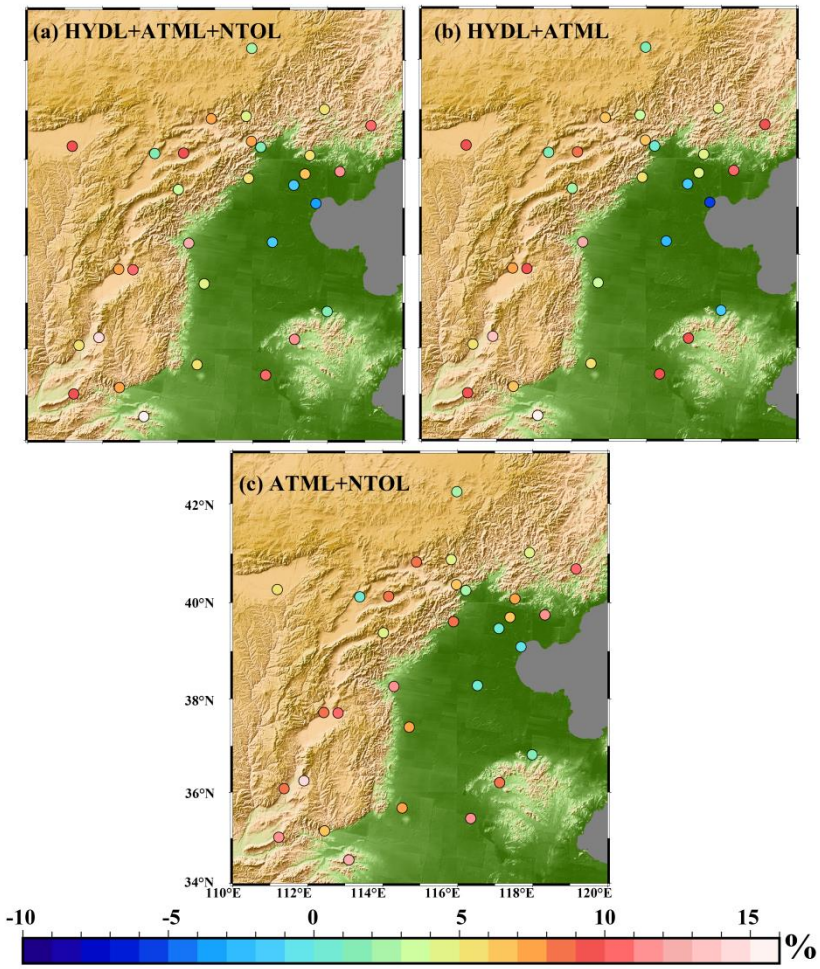

Fig. 7 RMS reduction results of the vertical GNSS time after deducting the deformation induced by the combined of HYDL+ATML+NTOL (a), HYDL+ATML (b), ATML+NTOL (c) from IMLS, respectively.

temporal and spatial resolutions as well as the HYDL models based on reanalysis data. The SLM data from IMLS is more suitable for studying the impact of HYDL on GNSS seasonal variations.

To evaluate the overall effect of surface mass loading on GNSS seasonal deformation, we calculated the RMS reduction value for combined SLM components (HYDL+ATML+NTOL, HYDL+ATML, and ATML+NTOL, respectively) using SLM data from IMLS, the results as shown in Figure 7. The RMS reduction value for HYDL+ATML+NTOL, HYDL+ATML, and ATML+NTOL correction vary from -3.8 % to 15.8 %, -5.3 % to 15.9 %, and -0.9 % to 14.8 %, respectively, with the average of 6.5 %, 5.7 % and 6.8 %. The RMS reduction value for HYDL+ATML+NTOL, HYDL+ATML, and ATML+NTOL at most stations (28, 27, 30) were positive, accounting for approximately 90 %, 87 %, and 97 % at all stations in North China.

3.3. THE IMPACT OF SURFACE MASS LOADING ON GNSS VELOCITY AND ITS UNCERTAINTY

We investigated the influence of surface mass loading on velocity and its uncertainty estimated from the GNSS time series, employing the Hector software with the maximum likelihood estimation method (Bos et al., 2013). The white noise (WN) model, characterized by random, uniformly distributed noises, was employed to estimate the velocity uncertainty from GNSS time series. The velocity uncertainty value estimated from GNSS ranges from 0.03 mm/a to 0.17 mm/a, with an average of 0.03 mm/a, implying that the velocity uncertainty based on the WN model was markedly overestimated at 31 stations in North China. It has demonstrated that the background spectrum of non-linear GNSS station position residuals closely adheres to a power-law process, referred to as flicker noise, pink noise or 1/f noise, with white noise predominating at the higher frequencies. Research has shown that the noise model integrating white noise and flicker noise (WN+FN) effectively characterizes the noise properties at most GNSS stations (He et al., 2019). Thus, we performed the WN+FN model to estimate the velocity and its uncertainty from the vertical GNSS time series before and after surface mass loading correction, the range of velocity and its uncertainty difference (Table 3) was 0.03~0.05 mm/a and 0~0.06 mm/a at all stations, respectively, with average of 0.04 mm/a for both,

Table 3 The difference in velocity and its uncertainty before and after SLM correction from IMLS at all stations in North China (unit: mm/a).

Station	velocity difference	velocity uncertainty difference	Station	velocity difference	velocity uncertainty difference
BJFS	0.04	0.05	NMZL	0.05	0.04
BJGB	0.04	0.03	SDJX	0.03	0.04
BJSH	0.04	0.03	SDZB	0.03	0.04
BJYQ	0.04	0.06	SXDT	0.04	0.01
HAHB	0.04	0.04	SXGX	0.04	0.05
HAJY	0.04	0.05	SXLF	0.04	0.04
HECC	0.04	0.05	SXLQ	0.04	0.05
HECD	0.04	0.03	SXTY	0.04	0.05
HECX	0.04	0.00	SXXX	0.03	0.05
HELQ	0.04	0.04	SXYC	0.04	0.04
HELY	0.03	0.04	TAIN	0.03	0.05
HETS	0.03	0.05	TJBD	0.04	0.04
HEYY	0.04	0.05	TJBH	0.03	0.04
HEZJ	0.05	0.05	TJWQ	0.04	0.00
JIXN	0.03	0.03	ZHNZ	0.04	0.04
NMTK	0.05	0.04			

implying that the effects of surface mass loading can be considered negligible when estimating the velocity and its uncertainty from the vertical GNSS time series in North China. These minimal shifts suggest that surface mass loading effects are insignificant for long-term velocity assessments in this region, possibly being overshadowed by tectonic deformation (uplift and subsidence) or other non-seasonal noise.

4. CONCLUSIONS

This study investigates seasonal deformation yielded by surface mass loading using GNSS and SLM data in North China. We calculated the RMS values, as well as the annual amplitudes and phases of deformations induced by surface mass loading. Furthermore, we performed a consistency analysis between GNSS time series and the deformations linked to HYDL, ATML, and NTOL. The primary conclusions are as follows.

The average RMS value of ATML deformation supplied by GFZ and IMLS was 4.18 mm and 4 mm, respectively, markedly exceeding the HYDL deformation values of 1.84 mm (GFZ) and 1.74 mm (IMLS). The average annual amplitude of GNSS time series was 4.6 mm, and the average annual amplitude of ATML deformation from GFZ and IMLS was 4.2 mm and 4.7 mm, respectively, aligning closely with GNSS. Moreover, a large discrepancy is evident in the HYDL phases between GFZ (67.9°) and IMLS (97°), indicating that ATML is the principal factor influencing seasonal fluctuations of GNSS time series in North China, but the effect of HYDL varies significantly depending on the SLM data.

The average RMS reduction value of ATML deformation collected from GFZ and IMLS was 5.9 % and 5.6 %, respectively, with positive reductions at 28 stations (90 % of total stations) from IMLS, indicating a robust corrective effect. Conversely, the average RMS reduction value of HYDL deformation was 0.99 % (GFZ) and -2.74 % (IMLS), with negative values observed at 81 % and 74 % at all stations, respectively, indicating that HYDL correction will increase the RMS value of the vertical GNSS time series in North China. In comparison to GFZ, SLM data from IMLS demonstrates superior consistency with GNSS time series, particularly for ATML, which outperforms HYDL and NTOL in aligning with seasonal variations.

The average of velocity and its uncertainty using the WN+FN model was 0.04 mm/a, this negligible difference indicates that surface mass loading has a minimal influence on the estimation of velocity and its uncertainty in North China.

ACKNOWLEDGMENTS

The GNSS time series data used in this paper is provided by GNSS data product service platform of China Earthquake Administration (http://data.earthquake.cn). The SLM data is provided by IMLS (http://massloading.net) and GFZ (http://rzvm115.gfz-potsdam.de:8080/repository).
This work was supported by the Open Funding of State Environmental Protection Key Laboratory of Monitoring for Heavy Metal Pollutants (Grant No. KLMHM202423).

REFERENCES

Bevis, M. and Brown, A.: 2014, Trajectory models and reference frames for crustal motion geodesy. J. Geod., 88, 3, 283–311. DOI: 10.1007/s00190-013-0685-5

Bos, M.S., Fernandes, R.M.S., Williams, S.D.P. and Bastos, L.: 2013, Fast error analysis of continuous GNSS observations with missing data. J. Geod., 87, 4, 351–360. DOI: 10.1007/s00190-013-0685-5

Carlson, G., Werth, S. and Shirzaei, M.: 2022, Joint inversion of GNSS and GRACE for terrestrial water storage change in California. J. Geophys. Res., Solid Earth, 127, 3, e2021JB023135. DOI: 10.1029/2021JB023135

Chanard, K., Avouac, J.P., Ramillien, G. and Genrich, J.: 2014, Modeling deformation induced by seasonal variations of continental water in the Himalaya region: Sensitivity to Earth elastic structure. J. Geophys. Res., Solid Earth, 119, 6, 5097–5113. DOI:10.1002/2013JB010451

Crossley, D.J., Murphy, J.T. and Liang, J.: 2023, Comprehensive analysis of superconducting gravimeter data, GPS, and hydrology modelling in support of lunar laser ranging at Apache Point Observatory, New Mexico. Geophys. J. Int., 232, 2, 1031–1065. DOI:10.1093/gji/ggac357

Dill, R.: 2008, Hydrological model LSDM for operational Earth rotation and gravity field variations. Sci. Tech. Rep. STR08/09. GFZ, Potsdam, Germany. DOI: 11.2312/GFZ.b103-08095

Dobslaw, H. and Thomas, M.: 2007, Simulation and observation of global ocean mass anomalies. J. Geophys. Res., Oceans, 112, C5. DOI: 10.1029/2006JC004035

Farrell, W.E. :1972, Deformation of the Earth by surface loads. Rev. Geophys., 10, 3, 761–797. DOI:10.1029/RG010i003p00761

Feng, T., Shen, Y., Chen, Q. and Wang, F.: 2022, Seasonal driving sources and hydrological-induced secular trend of the vertical displacement in North China. J. Hydrol.: Reg. Stud., 41, 101091. DOI: 10.1016/j.ejrh.2022.101091

Ferreira, L., Marotta, G.S., Madden, E.H., Horbe, A.M., Santos, R.V. and Costa, J.M.: 2021, Vertical displacement caused by hydrological influence in the Amazon Basin. J. Geophys. Res., Solid Earth, 126, 3, e2020JB020691. DOI:10.1029/2020JB020691

Gelaro, R., McCarty, W., Suárez, M.J., Todling, R., Molod, A., Takacs, L. et al.: 2017, The modern-era retrospective analysis for research and applications, version 2 (MERRA-2). J. Clim., 30, 14, 5419–5454.

Gobron, K., Rebischung, P., Van Camp, M., Demoulin, A. and de Viron, O.: 2021, Influence of aperiodic non-tidal atmospheric and oceanic loading deformations on the stochastic properties of global GNSS vertical land motion time series. J. Geophys. Res., Solid Earth, 126, 9, e2021JB022370. DOI:10.1175/JCLI-D-16-0758.1

Gu, Y., Yuan, L., Fan, D., You, W. and Su, Y.: 2017, Seasonal crustal vertical deformation induced by environmental mass loading in mainland China derived from GPS, GRACE and surface loading models. Adv. Space Res., 59, 1, 88–102. DOI: 10.1016/j.asr.2016.09.008

Haritonova, D.: 2021, Non-tidal loading of the Baltic Sea in Latvian GNSS time series. J. Appl. Geod., 15, 4, 293–304. DOI: 10.1515/jag-2021-0024

He, Y., Nie, G., Wu, S. and Li, H.: 2022, Comparative analysis of the correction effect of different environmental loading products on global GNSS coordinate time series. Adv. Space Res., 70, 11, 3594–3613. DOI: 10.1016/j.asr.2022.08.009

He, X., Bos, M.S., Montillet, J.P. and Fernandes, R.M.S.: 2019, Investigation of the noise properties at low frequencies in long GNSS time series. J. Geod., 93, 9, 1271–1282. DOI: 10.1007/s00190-019-01244-y

Heki, K. and Jin, S.: 2023, Geodetic study on earth surface loading with GNSS and GRACE. Satell. Navig., 4, 1, 24. DOI: 10.1186/s43020-023-00113-6

Hohensinn, R., Ruttner, P. and Bock, Y.: 2024, Sensitivity of GNSS to vertical land motion over Europe: effects of geophysical loadings and common-mode errors. J. Geod., 98, 7, 68. DOI: 10.1007/s00190-024-01856-z

Hu, S., Chen, K., He, X. et al.: 2025, Research on the impact of environmental loading on nonlinear variations of 3D coordinate time series of GNSS stations in Sichuan and Yunnan region. Acta Geod. Cartogr. Sin., 52, 5, 805–818. DOI: 10.11947/j.AGCS.2025.20240397

Huang, J., He, X., Hu, S. et al.: 2025, Impact of offsets on GNSS time series stochastic noise properties and velocity estimation. Adv. Space Res., 75, 4, 3397–3413. DOI: 10.1016/j.asr.2024.12.016

Jiang W., Wang, K., Li, Z., Zhou, X., Ma, Y. and Ma, J.: 2018, Prospect and theory of GNSS coordinate time series analysis. Geomatics and Information Science of Wuhan University, 43, 12, 2112–2123. DOI: 10.13203/j.whugis20180333

Jiang, Z., Hsu, Y.J., Yuan, L. and Huang, D.: 2021, Monitoring time-varying terrestrial water storage changes using daily GNSS measurements in Yunnan, southwest China. Remote Sens. Environ., 254, 112249. DOI: 10.1016/j.rse.2020.112249

Jiang, Z., Zhu, J., Guo, H., Qiu, K., Tang, M., Yang, X. and Liu, J.: 2024, South-to- North water diversion halting long-lived subsidence in Tianjin, North China Plain. Remote Sens., 16, 17, 3213. DOI: 10.3390/rs16173213

Li, S., Shen, W., Pan, Y. and Zhang, T.: 2020, Surface seasonal mass changes and vertical crustal deformation in North China from GPS and GRACE measurements. Geod. Geodyn., 11, 1, 46–55. DOI: 10.1016/j.geog.2019.05.002

Li, Z., Jiang, W., van Dam, T., Zou, X., Chen, Q. and Chen, H.: 2024, A review of surface mass distribution products, environmental loading products, and their contributions to nonlinear variations of global navigation satellite system (GNSS) coordinate time series. Engineering, 47, 26–37. DOI: 10.1016/j.eng.2024.09.001

Liang, H., Zhan, W. and Li, J.: 2021, Vertical surface displacement of mainland China from GPS using the multisurface function method. Adv. Space Res., 68, 12, 4898–4915. DOI: 10.1016/j.asr.2021.02.024

Liu, R., Li, J., Fok, H.S., Shum, C.K. and Li, Z.: 2014, Earth surface deformation in the north China plain detected by joint analysis of GRACE and GPS data. Sensors, 14, 10, 19861–19876. DOI: 10.3390/s141019861

Liu, N., Dai, W., Santerre, R. and Kuang, C.: 2018, A MATLAB-based Kriged Kalman Filter software for interpolating missing data in GNSS coordinate time series. GPS Solut., 22, 1, 25. DOI: 10.1007/s10291-017-0689-3

Liu, R., Zhong, B., Li, X., Zheng, K., Liang, H. et al.: 2022, Analysis of groundwater changes (2003–2020) in the North China Plain using geodetic measurements. J. Hydrol.: Reg. Stud., 41, 101085. DOI: 10.1016/j.ejrh.2022.101085

Longman, I.M.: 1963, A Green's function for determining the deformation of the Earth under surface mass loads: 2. Computations and numerical results. J. Geophys. Res., 68, 2, 485–496. DOI: 10.1029/JZ068i002p00485

Marsland, S.J., Haak, H., Jungclaus, J.H., Latif, M. and Röske, F.: 2003, The Max- Planck-Institute global ocean/sea ice model with orthogonal curvilinear coordinates. Ocean Model., 5, 2, 91–127. DOI: 10.1016/S1463-5003(02)00015-X

Martens, H.R., Argus, D.F., Norberg, C., Blewitt, G., Herring, T.A. et al.: 2020, Atmospheric pressure loading in GPS positions: Dependency on GPS processing methods and effect on assessment of seasonal deformation in the contiguous USA and Alaska. J. Geod., 94, 1–22. DOI: 10.1007/s00190-020-01445-w

Montecino, H.D., Pontes, J.I., Gonçalves, R.M. et al.: 2025, The relation between vertical crustal deformation and hydrological changes in the São Francisco River basin from 2014 to 2024. Earth Sci. Inform., 18, 3, 1–16. DOI: 10.1007/s12145-025-01908-8

Niu, Y., Wei, N., Li, M., Rebischung, P., Shi, C. and Chen, G.: 2022, Quantifying discrepancies in the three-dimensional seasonal variations between IGS station positions and load models. J. Geod., 96, 4, 31. DOI: 10.1007/s00190-022-01618-9

Pan, Y., Shen, W.B., Hwang, C., Liao, C., Zhang, T. and Zhang, G.: 2016, Seasonal mass changes and crustal vertical deformations constrained by GPS and GRACE in Northeastern Tibet. Sensors, 16, 8, 1211. DOI: 10.3390/s16081211

Peng, Y., Chen, G., Chao, N., Wang, Z., Wu, T. and Luo, X.: 2024, Detection of extreme hydrological droughts in the Poyang lake basin during 2021–2022 using GNSS-derived daily terrestrial water storage anomalies. Sci. Total Environ., 919, 170875. DOI: 10.1016/j.scitotenv.2024.170875

Sauveur, R., Tabibi, S. and Francis, O.: 2024, Hydrological loading in GNSS vertical coordinate time series on the Island of Haiti. Pure Appl. Geophys., 181, 12, 3591–3604. DOI: 10.1007/s00024-024-03606-w

Su, G. and Zhan, W.: 2021, Seasonal and long-term vertical land motion in Southwest China determined using GPS, GRACE, and surface loading model. Earth Planets Space, 73, 1–14. DOI: 10.1186/s40623-021-01459-4

Suraci, S., de Oliveira, L., Klein, I. et al.: 2025, A meta-classification-based approach for outlier identification in GNSS networks. GPS Solut., 29, 1, 21. DOI: 10.1007/s10291-024-01775-8

Tang, M., Yuan, L., Jiang, Z., Yang, X., Li, C. and Liu, W.: 2023, Characterization of hydrological droughts in Brazil using a novel multiscale index from GNSS. J. Hydrol., 617, 128934. DOI: 10.1016/j.jhydrol.2022.128934

Van Dam, T., Collilieux, X., Wuite, J., Altamimi, Z. and Ray, J.: 2012, Nontidal ocean loading: amplitudes and potential effects in GPS height time series. J. Geod., 86, 1043–1057. DOI: 10.1007/s00190-012-0564-5

Wang, L., Chen, C., Zou, R., Du, J. and Chen X.: 2014, Using GPS and GRACE to detect seasonal horizontal deformation caused by loading of terrestrial water: A case study in the Himalayas. Chin. J. Geophys., 57, 6, 1792–1804, (in Chinese). DOI: 10.6038/cjg20140611

Wang, L., Chen, C., Du, J. and Wang, T.: 2017, Detecting seasonal and long-term vertical displacement in the North China Plain using GRACE and GPS. Hydrol. Earth Syst. Sci., 21, 6, 2905–2922. DOI: 10.5194/hess-21-2905-2017

Wang, J., Fan, W., Jiang, W., Li, Z., Liu, T. and Chen, Q.: 2025, Investigating source mechanisms for nonlinear displacement of GNSS using environmental loads. Remote Sens., 17, 6, 989. DOI: 10.3390/rs17060989

Wang, J., Ding, K., Chen, X., Guo, R. and Sun, H.: 2023, Influence of South-to-North water diversion on land subsidence in North China Plain revealed by using geodetic measurements. Remote Sens., 16, 1, 162. DOI: 10.3390/rs16010162

Wu, M., Wu, J., Liu, J., Wu, J. and Zheng, C.: 2015, Effect of groundwater quality on sustainability of groundwater resource: A case study in the North China Plain. J. Contam. Hydrol., 179, 132–147. DOI: 10.1016/j.jconhyd.2015.06.001

Xue, L., Fu, Y. and Martens, H.R.: 2021, Seasonal hydrological loading in the Great Lakes region detected by GNSS: A comparison with hydrological models. Geophys. J. Int., 226, 2, 1174–1186. DOI: 10.1093/gji/ggab158

Zhao, B., Huang, Y., Zhang, C., Wang, W., Tan, K. and Du, R.: 2015, Crustal deformation on the Chinese mainland during 1998–2014 based on GPS data. Geod. Geodyn., 6, 1, 7–15. DOI: 10.1016/j.geog.2014.12.006

Zhang, R., Peng, Y., Chao, N., Ou, Q., Chen, G. et al.: 2025, A rapid increase of groundwater in 2021 over the North China Plain from GPS and GRACE observations. GPS Solut., 29, 1, 1–20. DOI: 10.1007/s10291-024-01794-5

Zhang, J., Li, Z., Zhang, P., Yang, F., Wu, J., Liu, X. et al.: 2023, Assessing the nonlinear changes in global navigation satellite system vertical time series with environmental loading in Mainland China. Remote Sens., 15, 16, 4115. DOI: 10.3390/rs15164115

Zhou, Y., He, X., Montillet, J.P. et al.: 2025, An improved ICEEMDAN-MPA-GRU model for GNSS height time series prediction with weighted quality evaluation index. GPS Solut., 29, 3, 1–19. DOI: 10.1007/s10291-025-01867-z